IIETA International Information and Engineering Technology Association
Advancing the World of Information and Engineering

Traitement du Signal
Vol. 42, No. 6, December, 2025, pp. 3263-3276
Journal homepage: http://iieta.org/journals/ts

A Robust Multi-Transform Watermarking Scheme for Medical Images Using DTCWT, DCT, and SVD

Ali Kouadri[1], Abdelhalim Rabehi[1], Ali Benziane[1], Abdelaziz Rabehi[1*], Hamza Kheddar[2], Amel Ali Alhussan[3], Doaa Sami Khafaga[3], El-Sayed M. El-Kenawy[4,5]

[1] Laboratory of Telecommunications and Smart Systems, Faculty of Sciences and Technologies, University of Djelfa, Djelfa 17000, Algeria
[2] LSEA Laboratory, Electrical Engineering Department, Faculty of Technology, University of Medea, Medea 26000, Algeria
[3] Department of Computer Sciences, College of Computer and Information Sciences, Princess Nourah Bint Abdulrahman University, Riyadh 11671, Saudi Arabia
[4] Department for Communications and Electronics, Delta Higher Institute of Engineering and Technology, Mansoura 35511, Egypt
[5] Applied Science Research Center, Applied Science Private University, Amman 11937, Jordan

Corresponding Author Email: abdelaziz.rabehi@univ-djelfa.dz

https://doi.org/10.18280/ts.420618

Received: 1 August 2025
Revised: 26 August 2025
Accepted: 23 September 2025
Available online: 31 December 2025

Keywords:
watermarking, DTCWT, DCT, SVD, medical image, robustness, embedding capacity, imperceptibility

ABSTRACT

A novel watermarking framework integrates the Dual-Tree Complex Wavelet Transform (DTCWT), Discrete Cosine Transform (DCT), and Singular Value Decomposition (SVD) techniques to protect medical image integrity. The method applies hierarchical embedding where both host image and watermark undergo DTCWT decomposition, followed by DCT processing and SVD of selected high-frequency subbands. Watermark singular values are embedded into corresponding host image values, enhancing robustness while preserving diagnostic quality. Testing on 512×512 images across X-ray, CT, MRI, and ultrasound modalities achieves PSNR values of 64.20-64.67dB, SSIM exceeding 0.9992, and NC consistently above 0.99999. Evaluation against 23 attack types demonstrates exceptional resilience, with 15-21dB improvements over existing methods. This multi-transform approach optimizes embedding capacity, attack resistance, and visual imperceptibility, addressing essential criteria for medical image watermarking applications.

1. INTRODUCTION

In the context of telemedicine based on medical imaging, unauthorized access to or modification of diagnostic images poses significant medical and legal risks, as it may lead to diagnostic errors and inappropriate treatments [1]. Moreover, the secure transmission and exchange of radiological data between healthcare institutions and medical professionals is a key factor in promoting multidisciplinary collaboration and obtaining specialized consultative expertise [2].

The preservation of healthcare information integrity necessitates adherence to three fundamental pillars: confidentiality, reliability, and availability. Confidentiality encompasses the implementation of comprehensive privacy safeguards and the establishment of stringent access controls to protect sensitive medical data from unauthorized disclosure [3]. Reliability constitutes the assurance of information authenticity and immutability, guaranteeing that data remains uncompromised and forensically verifiable throughout its lifecycle [4]. Availability guarantees that authorized personnel can consistently access vital information, preventing service interruptions that might hinder clinical decisions [5]. Consequently, the implementation of robust mechanisms to safeguard both the integrity and provenance of medical imaging data emerges as an imperative priority within contemporary healthcare infrastructure [6].

Modern healthcare infrastructures rely on multi-layered security architectures that encompass access control protocols, firewalls, anti-malware solutions, intrusion detection systems, steganographic techniques, and cryptographic frameworks. Steganographic methods operate based on information concealment models, prioritizing covert data protection over transparent accessibility. Although cryptographic algorithms are the primary tools for ensuring the integrity of medical data. They possess an inherent vulnerability: once decrypted, the previously protected information becomes susceptible to unauthorized manipulation [7].

In contrast, digital watermarking facilitates image authentication and provenance tracking, enabling detection of unauthorized modifications and source verification. Such functionality holds exceptional significance for safeguarding the fidelity of medical imaging data across all operational phases—spanning initial capture, archival processes, data transfer, and diagnostic evaluation [1]. Digital watermarking technology embeds identifying markers within host images while ensuring negligible and undetectable alterations, thereby preserving visual fidelity. Following embedding, the marked image undergoes transmission to designated receivers who

authenticate its legitimacy through watermark extraction and verification processes [8]. Watermarking extraction occurs through blind, semi-blind, or non-blind methods, differentiated by original image dependency. While visible watermarks exist, invisible implementations dominate due to superior security and copyright enforcement. These invisible techniques split between robust (ownership protection) and fragile (tamper detection) applications [9]. Watermarking operates through spatial domain (direct pixel embedding via Local Binary Pattern (LBP) [10]. Least Significant Bit (LSB) [11], Direct Sequence Spread Spectrum (DSSS) [12], Intermediate Significant Bit (ISB) [13], and Pixel Value Differencing (PVD) [14] or frequency domain (coefficient modification post-transformation) [7, 15] techniques. Frequency-domain techniques embed watermarks within transformed image representations rather than raw pixel data [9]. These approaches utilize various mathematical transformations including Redundant Discrete Wavelet Transform (RDWT) [16], Discrete Wavelet Transform (DWT) [15, 17, 18], Discrete Cosine Transform (DCT) [15, 17, 19], Lifting Wavelet Transform (LWT) [7, 20, 21] and Integer Wavelet Transform (IWT) [22, 23]. Operating in the transform domain offers superior embedding efficiency and enhanced resistance to attacks compared to spatial methods. Recent advances have explored hybrid strategies that synergistically combine multiple transforms, resulting in improved visual transparency and strengthened security against malicious attacks [24].

This study aims to create an effective watermarking solution for medical imagery that balances maintaining image fidelity with strengthening protection against different attacks. The proposed approach combines three key transformation methods Dual-Tree Complex Wavelet Transform (DTCWT), Discrete Cosine Transform (DCT), and Singular Value Decomposition (SVD) to build a unified security architecture. The DTCWT provides quasi shift-invariant properties and improved directional discrimination, producing several complex-valued subbands that substantially expand the embedding potential [24]. Meanwhile, the DCT enhances durability against compression-related distortions [25], and the SVD utilizes its geometric stability properties to reinforce resistance across various attack conditions [7]. This integrated multi-transform strategy simultaneously enhances embedding volume, attack tolerance, and visual imperceptibility, thus fulfilling the essential demands of watermarking in medical imaging applications.

2. RELATED WORK

Transform-based techniques have attracted substantial research attention for their dual achievement of robustness and imperceptibility, proving especially valuable in medical imaging where data authenticity and integrity demand absolute protection. In watermarking systems, robustness remains the critical challenge. Hybrid strategies address this by combining complementary strengths across different domains, creating comprehensive defense against attacks. A relevant contribution in this domain comes from Sundhararaj et al. [26] who developed a watermarking technique that integrates DWT, DCT, and SVD transformations to mitigate False Positive Problem (FPP) commonly encountered in watermarking systems. This method is computationally expensive due to its use of three transforms, making it impractical for real-time applications. Additionally, its robustness is questionable as it was not adequately tested against common image processing steps like compression or resizing. Latreche et al. [7] developed a two-tier watermarking approach aimed at protecting both the integrity and security of medical images throughout the transmission process. Their technique employs multiple transformations including the LWT, Hessenberg Decomposition (HD), and SVD, alongside chaotic encryption based on the Logistic map function. Its main drawbacks are high computational complexity, sensitivity to parameter tuning, the potential to create visual artifacts, and the inherent unreliability of its chaotic encryption component. Naima et al. [1] developed a watermarking technique operating in the frequency domain that integrates the Fractional Discrete Cosine Transform (FDCT), Radon Transform, and Schur decomposition methodologies. Its primary weaknesses are computational inefficiency, poor robustness against speckle noise, and the challenge of balancing imperceptibility with performance. Sayah et al. [27] implemented a medical image watermarking approach utilizing IWT combined with SVD. However, this method exhibits several shortcomings, including compromised visual quality when handling large payload capacities, lack of validation across databases other than ODIR, computational complexity that prevents real-time implementation, and uncertain resilience to significant geometric distortions such as cropping and rotation operations. Basit et al. [28] proposed a reversible encryption and data hiding method combining DWT and SVD for secure medical image transmission. The scheme ensures imperceptibility and robustness but suffers from high computational cost due to multiple SVD operations, limiting real-time applicability. In a related effort, Shubuh et al. [29] created a combined IWT-DCT-SVD watermarking system designed for copyright protection purposes. While the method showed resilience to common attacks like compression and noise, it suffers from significant drawbacks. Its performance degrades considerably against histogram equalization and sharpening attacks. Furthermore, its evaluation on a limited set of grayscale images and sensitivity to parameter tuning question its practical applicability in real-time or diverse imaging scenarios. The hybrid DWT/LWT-DCT-SVD watermarking method by Awasthi and Srivastava [30] uses PSO and JAYA optimization to find an embedding factor. However, this approach is limited by visual artifacts and the significant computational load of the iterative optimizers. Fares et al. [31] introduced two watermarking approaches that integrate discrete cosine transform (DCT) with Schur decomposition. While these techniques achieve reasonable equilibrium between robustness and imperceptibility, they remain susceptible to specific attack types, especially noise interference and compression operations. Meanwhile, Anand and Singh [32] created a dual watermarking system for medical CT scan images employing RDWT and Randomized singular value decomposition (RSVD). Nevertheless, this approach exhibits substantially elevated BER values when subjected to sharpening, histogram equalization, and cropping operations, revealing weak resistance to these frequently encountered image processing techniques. Khare et al. [4] proposed a method that integrates DWT with Homomorphic Transforms (HT) and SVD, using Arnold transforms to scramble the watermark. While this approach demonstrates robustness against common attacks, it struggles with imperceptibility, especially in medical images. Lastly, Kanwal et al. [33] proposed a hybrid blind watermarking method

combining DWT and DCT with an adaptive scaling factor to embed imperceptible watermarks in medical images. The technique achieved high robustness against noise and compression, though its computational cost may limit real-time use.

3. USED TRANSFORM DOMAINS

3.1 Dual tree complex wavelet transform

Among advanced transformation techniques, DTCWT distinguishes itself by integrating the favorable attributes of both DWT and CWT transforms. This transformation provides exact reconstruction capabilities, efficient computation, near shift-invariance properties, and selective directional filtering mechanisms [34]. Unlike the single-tree architecture of conventional DWT, the DTCWT implements a dual-tree structure that creates two separate coefficient sets, which are then merged to form complex-valued coefficients. In practice, DTCWT employs two separates real DWTs using different filter banks, where one DWT generates the real component of the transform and the other produces the imaginary component [24]. This transform has proven successful in various image processing applications such as classification, denoising, segmentation, enhancement procedures, and watermark insertion. Within watermarking contexts, the quasi shift-invariant property of DTCWT offers significant benefits, enabling embedded information to withstand geometric transformations while maintaining minimal distortion [35]. Moreover, the transform's superior perceptual features, particularly through improved directional analysis of high-frequency components compared to DWT, facilitate the embedding of more imperceptible watermarks. When applied to two-dimensional images, DTCWT generates distinct coefficient structures at each decomposition level, comprising two complex-valued low-frequency subbands and six complex-valued high-frequency subbands. These high-frequency components are derived from six directionally-selective filters oriented at ±15°, ±45°, and ±75° angles [36]. Figure 1 demonstrates how the initial decomposition level of an input image through DTCWT produces this particular collection of subbands. The complex-valued coefficients obtained from this decomposition process can be mathematically expressed as [24]:

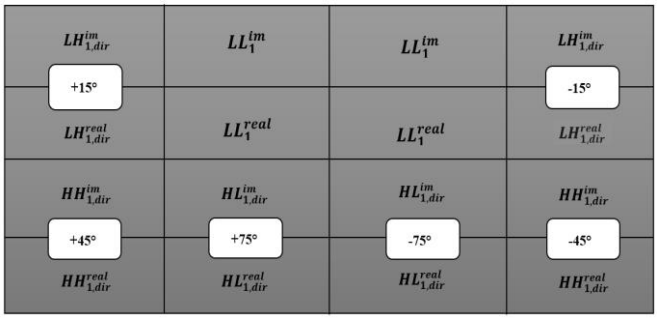

Figure 1. The DTCWT's first-level decomposition subbands

$$Z_{Lev,dir} = Y^{real}_{Lev,dir} + jY^{im}_{Lev,dir} \quad (1)$$

where, Lev refers to the decomposition level, while dir signifies the directional angles of ±15°, ±45°, and ±75°, which characterize the complex HF components (indexed dir from 1 to 6). The $Y^{real}_{Lev,dir}$ and $jY^{im}_{Lev,dir}$ terms denote the real and imaginary portions, respectively, collected during the DTCWT's dual-tree decomposition [24].

3.2 Discrete cosine transform

Image processing applications, especially JPEG compression systems, rely heavily on a core mathematical procedure known as the Discrete Cosine Transform (DCT). Through its two-dimensional implementation (2D DCT), this technique enables the transformation of M×N spatial image data into its equivalent frequency domain representation according to the mathematical formulation [8]:

$$T(l,m) = b(l)b(m)\sum_{p=0}^{M-1}\sum_{k=0}^{N-1} t(p,k) \times \cos\left(\frac{(2p+1)l\pi}{2N}\right)\times\cos\left(\frac{(2k+1)m\pi}{2N}\right) \quad (2)$$

Within this mathematical framework, $t(p, k)$ denotes the intensity value of a pixel located at position (p, k) in the source image, while the output coefficient at frequency coordinates (u, v) is given by the transformed value. The normalization parameters $b(u)$ and $b(v)$ serve as scaling constants that ensure proper mathematical consistency, established as [37]:

$$b(l) = \begin{cases} \sqrt{\frac{1}{M}} & \text{for l} = 0 \\ \sqrt{\frac{2}{M}} & \text{for l} = 1,2,\dots,M-1 \end{cases} \quad (3)$$

$$b(m) = \begin{cases} \sqrt{\frac{1}{N}} & \text{for m} = 0 \\ \sqrt{\frac{2}{N}} & \text{for m} = 1,2,\dots,N-1 \end{cases}$$

Of course, we often need to get the image back, that's where the 2D-IDCT comes in. It essentially reverses the 2D-DCT process, transforming the frequency data $T(l,m)$ back into the original spatial pixel values $t(p,k)$. You calculate it like this [8]:

$$t(p,k) = \sum_{l=0}^{M-1}\sum_{m=0}^{N-1} b(l)b(m)\,T(l,m) \times \cos\left(\frac{(2p+1)l\pi}{2N}\right) \times\cos\left(\frac{(2k+1)m\pi}{2N}\right) \quad (4)$$

3.3 Singular value decomposition

A fundamental matrix factorization technique, Singular Value Decomposition (SVD) is widely acknowledged as one of the most powerful linear algebra methodologies. This approach enables the identification of crucial structural characteristics within matrices and finds particularly valuable applications in image analysis and related fields. The core principle involves transforming an original matrix into three distinct matrix components, thereby creating a condensed representation of the source matrix's key elements [30].

Given any matrix (or image) I, SVD decomposes it into three distinct matrices namely U, S, and V which satisfy the relation [38]:

$$A = U * S * V^t = \sum_{i=1}^{n} (\sigma_i * u_i * v_i^t) \quad (5)$$

Matrix S exhibits a diagonal structure containing the singular values σ_i [38]:

$$S = \begin{bmatrix} \sigma_i & \cdots & 0 \\ \vdots & \ddots & \vdots \\ 0 & \cdots & \sigma_n \end{bmatrix} \quad (6)$$

The SVD components include orthogonal matrices U and V, whose columns are the eigenvectors of II^T and I^TI, respectively. These vectors expose the image's key geometric features. The diagonal matrix $S = diag(\sigma_i \ldots \sigma_n)$ contains the singular values arranged in decreasing order, representing the significance of each corresponding vector [7]. In the context of image processing, particularly for digital watermarking applications, SVD holds a central position. Its advantages encompass the identification of dominant visual components, satisfactory stability, resistance to signal processing transformations, and efficient representation of visual information. Minor adjustments to singular values maintain the perceptual quality of the image. Furthermore, this methodology imposes no dimensional restrictions on the input image matrix [39].

4. SUGGESTED APPROACH

Our watermarking method works in two main steps: embedding the watermark and then extracting it. The core innovation combines three techniques: DTCWT, DCT, and SVD. This combination significantly boosts the watermark's capacity (how much data you can hide), robustness (resistance to tampering), and imperceptibility (how hard it is to see), all while maintaining the original host image quality. This holds true even when the image faces common attacks like geometric distortions or signal processing operations. We chose DTCWT specifically because it's a powerful upgrade to the standard DWT. It offers key advantages: it's nearly shift-invariant, excels at capturing directional details in images (especially important in 2D), and handles geometric attacks very effectively. Another major benefit is how DTCWT processes the cover image [40]. The transform partitions the host image into two complex low-frequency subbands (containing real and imaginary components) and six complex high-frequency subbands. This detailed decomposition creates many more potential hiding places, directly increasing the amount of data we can embed [27].

4.1 The embedding process

In this section, we've walked through our watermark embedding process (visualized in Figure 2) and detailed in Algorithm 1. Like most watermarking methods, our approach takes two key inputs: the cover image (labeled C) sized M×M pixels and the watermark image (labeled W) sized N×N pixels.

(1) Perform the DTCWT to both the host image sized M×M and the watermark image sized N×N. Following DTCWT decomposition, each image is separated into six distinct complex high-frequency sub-bands.

(2) Subsequently, we implement a DCT on the high-frequency subbands derived from the DTCWT decomposition of both the host and watermark images. In particular, we utilize the subband from the (3rd orientation, 2nd tree, real component) to produce the corresponding DCT coefficients.

(3) Perform Singular Value Decomposition on the cover image's DCT coefficients (yielding U_C, S_C, V_C^T) and the watermark's coefficients (yielding U_W, S_W, V_W^T).

$$Im = U_C \times S_C \times V_C^T \quad (7)$$

$$Wat = U_W \times S_W \times V_W^T \quad (8)$$

(4) The singular value decomposition (SVD) coefficients undergo modification according to the formula [41]:

$$S = S_c + \alpha\, S_W \quad (9)$$

In this formulation α represents a scaling parameter that controls the trade-off between watermark invisibility in the host image and robustness against different attack types.

(5) Following this modification, SVD is performed on the modified coefficients S to derive the updated DTCWT coefficients for the host image.

(6) Computing the inverse discrete cosine transform of the altered DTCWT coefficients, followed by applying the inverse DTCWT to obtain the watermarked image.

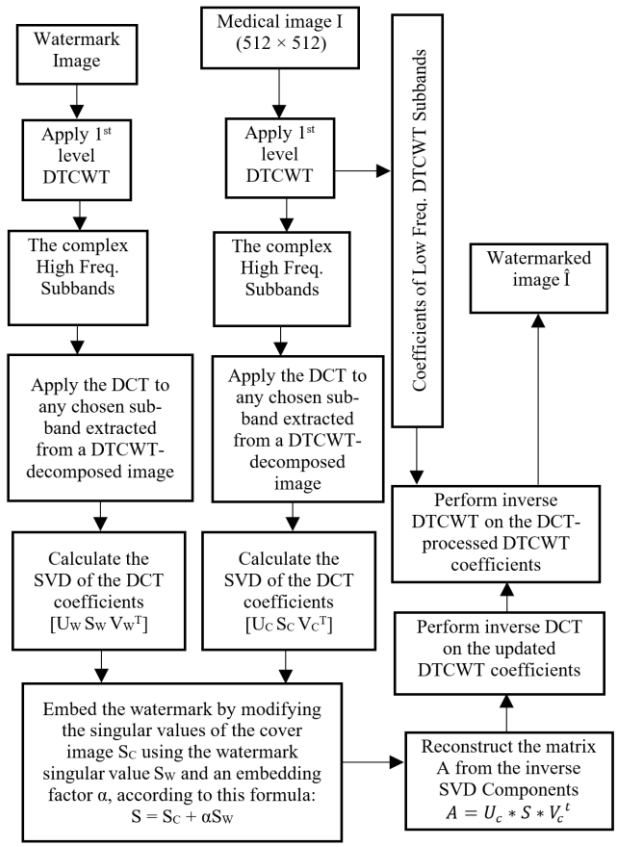

Figure 2. The embedding process

Algorithm 1: Watermarking embedding procedure
function Watermark Embedding
Parameters: (I, W, α)
Input: Cover image I; Watermark W; Gain factor (α).
Output: Watermarked Image (I^*).
Start
1: $wt = dddtree2('cplxdt', I, 1^{st}\ level, 'dtf3');$
2: $HF = wt.cfs\{1\}(:,:,3,1,2);$
2: $HF^C = dct2(HF);$
3: $U_C S_C V_C^T = svd(HF^C);$
4: $U_W S_W V_W^T = svd(HF^W);$

5: $S = S_C + \alpha S_W$;
6: $A = U_C\ S\ V_C^T$;
7: $HF^{\nabla} = idct2(A)$;
8: $wt.cfs\{1\}(:,:,3,1,2) = HF^{\nabla}$;
9: $\hat{I} = idddtree2(wt)$;
Return (Î)
End.

4.2 The extraction process

Watermark extraction (described below) is depicted in Figure 3 and outlined in Algorithm 2. The method processes watermarked image C' (m×m) to output extracted watermark W' (n×n).

(1) Perform DTCWT decomposition to the watermarked image, generating six complex high-frequency subbands. Then select the exact same directional subband used during the embedding process.

(2) Calculate the DCT coefficients from the chosen DTCWT subband of the watermarked image.

(3) Take the DCT coefficients and compute their Singular Value Decomposition. This factorization produces three matrices: $U_{w\prime}$, $S_{w\prime}$, and $V_{w\prime}^T$.

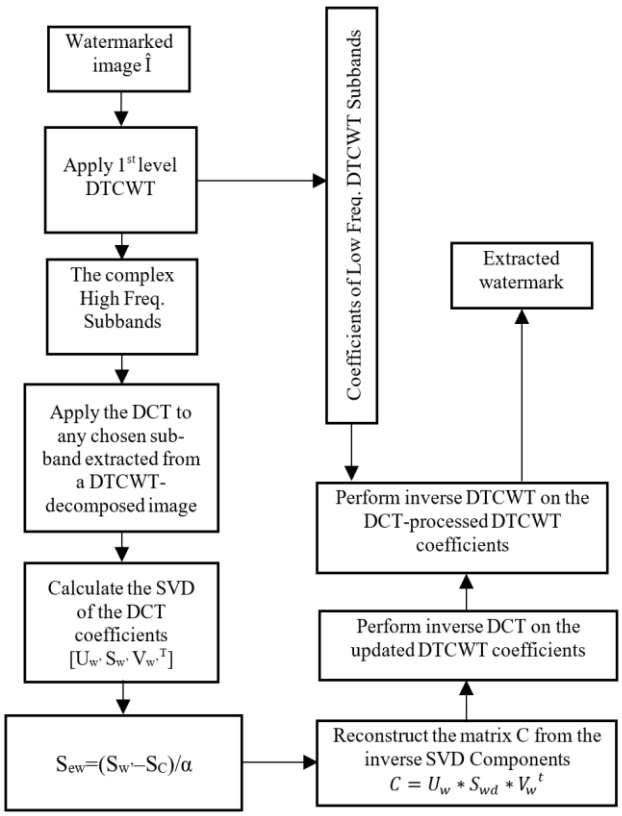

Figure 3. The extraction process

Modify the singular values using the inversion of the embedding operation [41]:

$$S_{wd} = (S_{w\prime} - S_c)/\alpha \tag{10}$$

Reconstruct the matrix C from the inverse SVD Components:

$$C = U_w * S_{wd} * V_w{}^t \tag{11}$$

Transform the modified coefficients through inverse DCT, then process the output with inverse DTCWT. This yields the recovered watermark image.

Algorithm 2: Watermarking extracting procedure
function Watermark Extraction
Parameters: (Î, α)
Input: Watermarked image (Î); Gain factor (α).
Output: Extracted Watermark (W^*).
Start
1: $wt^{\nabla} = dddtree2('cplxdt', \hat{I}, 1^{st}\ level, 'dtf3')$;
2: $HF^{\nabla} = wt^{\nabla}.cfs\{1\}(:,:,3,1,2)$;
2: $HF^* = dct2(HF^{\nabla})$;
3: $U_{W\prime}S_{W\prime}V_{W\prime}^T = svd(HF^*)$;
4: $S_{wd} = (S_{W\prime} - S_C)/\alpha$;
5: $C = U_W\ S_{wd}\ V_W^T$;
6: $HF^* = idct2(C)$;
7: $wt^{\nabla}.cfs\{1\}(:,:,3,1,2) = HF^*$;
8: $\hat{W} = idddtree2(wt^{\nabla})$;
Return (Ŵ)
End.

4.3 Performance assessment metrics

The efficacy of watermarking systems is gauged by quantitative measures that assess the visual quality of modified images.

Mean Square Error (MSE): This metric measures the mean error between corresponding pixels of two images by computing the average of squared pixel value differences, as demonstrated Eq. (12). A minimum MSE value indicates a higher degree of similarity and less embedding-induced distortion [7].

$$MSE(Imo, Imw) = \frac{1}{M^2}\sum_{i=1}^{M}\sum_{j=1}^{M}\left(Imo_{i,j} - \mathrm{Imw}_{i,j}\right)^2 \tag{12}$$

In this equation, Imo signifies the source image, Imw indicates the watermarked variant, and M represents the image size.

Peak Signal-to-Noise Ratio (PSNR): This metric assesses watermarked image quality by contrasting the maximum achievable signal strength against the noise power, which stems from the MSE calculation. According to Eq. (13), elevated PSNR values indicate superior visual fidelity and enhanced watermark transparency. In this context, 'Max' denotes the highest possible pixel intensity within the image (such as 255 for 8-bit imagery) [8].

$$PSNR(Imo, Imw) = 10 \times log_{10}\left(\frac{Max^2}{MSE(Imo, Imw)}\right) \tag{13}$$

Structural Similarity Index Measure (SSIM): Rather than relying on pixel-level comparisons, this metric evaluates perceived structural information changes between two images by analyzing luminance, contrast, and structural components. SSIM values span from -1 to 1, with a score of 1 indicating perfect structural equivalence between the images. The calculation process is outlined in Eq. (14).

$$SSIM(Imo, Imw) = \frac{2\mu_{Imo}\mu_{Imw} + v_1}{\mu_{Imo}^2 + \mu_{Imw}^2 + v_1} \times \frac{2\sigma_{ImoImw} + v_2}{\sigma_{Imo}^2 + \sigma_{Imw}^2 + v_2} \tag{14}$$

Within the SSIM formula, μ_{Imo} and μ_{Imw} represent the

average intensity values, whereas σ^2_{Imo} and σ^2_{Imw} denote the variance measures for the source and watermarked images, respectively. The term $\sigma_{Imo\mathrm{Imw}}$ represents their covariance, and v_1 along with v_2 serve as small stabilization constants that prevent division issues [7].

For evaluating the watermark's resistance to attacks, the correlation between the embedded watermark W_{Emb} and the recovered watermark W_{Ext} is determined. This assessment utilizes the Normalized Correlation Coefficient (NC), a widely-used metric for evaluating robustness:

$$NC(W_{Emb}, W_{Ext}) = \frac{\sum_{i=1}^{n}\sum_{j=1}^{n} W_{Emb_{i,j}} \times W_{Ext_{i,j}}}{\sqrt{\sum_{i=1}^{n}\sum_{j=1}^{n} W^2_{Emb_{i,j}}}\sqrt{\sum_{i=1}^{n}\sum_{j=1}^{n} W^2_{Ext_{i,j}}}} \quad (15)$$

Here, $W_{Emb_{i,j}}$ and $W_{Ext_{i,j}}$ are the respective pixel intensities. An NC of 1 indicates perfect recovery, whereas diminished values reflect reduced resilience to image manipulations [7].

5. EXPERIMENTAL RESULTS AND DISCUSSION

The evaluation of the proposed watermarking approach focuses on imperceptibility, robustness, and comparative analysis. Experiments were conducted on diverse medical imaging types, including X-ray, CT, MRI, and Ultrasound (Figure 4), with all images standardized to 512 × 512 pixels and obtained from different datasets [42, 43]. Institutional logos and other watermark patterns (Figure 5) [7] were embedded at multiple resolutions (256 × 256, 128 × 128, 64 × 64). The experiments were conducted using MATLAB R2022b on a Windows 10 platform equipped with an Intel Core i5 processor (3.2GHz) and 8GB of RAM.

5.1 Gain factor selection

The gain factor α controls the balance between the imperceptibility and watermark robustness: reducing α minimizes image distortion but compromises watermark strength, while increasing α enhances durability but degrades visual quality, as demonstrated in Figure 6. To determine the ideal value, we tested α values from 0.1 to 1.0 in 0.1 increments, measuring mean PSNR and NC values across various medical image types. We established two criteria: (I) visual quality requirements with PSNR ≥ 64dB to maintain diagnostic integrity, and (II) durability requirements with NC ≥ 0.999982 under Gaussian noise conditions (σ^2 = 0.001). Analysis revealed that only the 0.5-0.6 range met both requirements simultaneously. Values below 0.5 provided inadequate durability, while values above 0.6 produced noticeable quality loss. Consequently, α = 0.6 was chosen as the standard embedding parameter, offering optimal equilibrium between imperceptibility and watermark robustness for medical imaging applications.

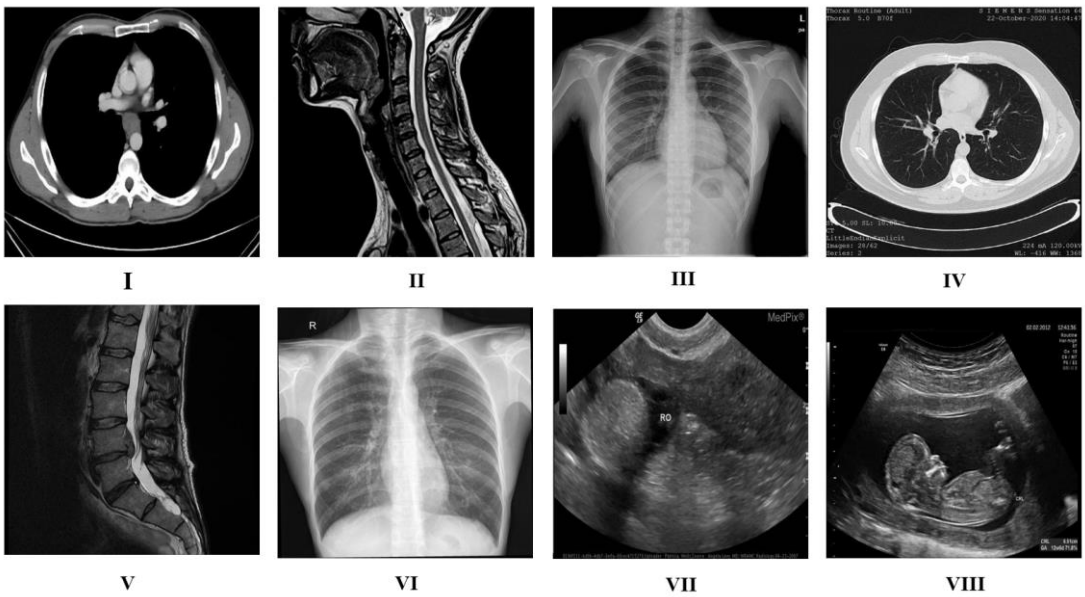

Figure 4. Sample medical imaging modalities: (I) Thoracic1_CT, (II) Spinal_MRI, (III) Chest1_X-ray, (IV) Thoracic2_CT, (V) Lumbar_MRI, (VI) Chest2_X-ray, (VII) Ovarian_Ultrasound, (VIII) Fetal_Ultrasound

Figure 5. Test watermarks

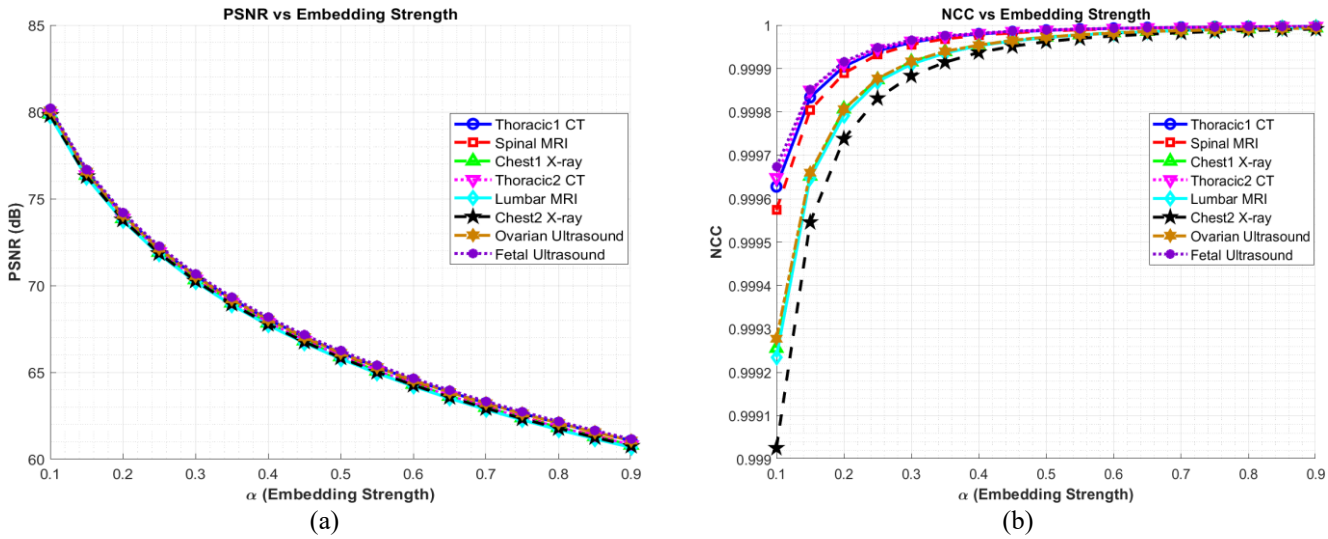

Figure 6. (a) PSNR values of the watermarked images in relation to the scaling parameter (α) and (b) Performance of the recovered watermark relative to the scaling parameter α following Gaussian noise (σ^2=0.001)

5.2 Imperceptibility analysis

We assess the effectiveness of the proposed scheme in this section by focusing on its main performance attributes: imperceptibility and robustness. Our assessment methodology includes both a qualitative visual review and a rigorous quantitative evaluation. To ensure the watermark does not compromise data confidentiality, it must remain undetectable to the human eye. We adhere to widely accepted quality benchmarks to verify this: an image is considered to have high fidelity when its PSNR is 29dB or greater [44], while an SSIM value of 0.90 or higher is another crucial benchmark for confirming that perceptual quality is maintained [45]. In contrast, significant distortion is present if the PSNR drops below 25dB [44].

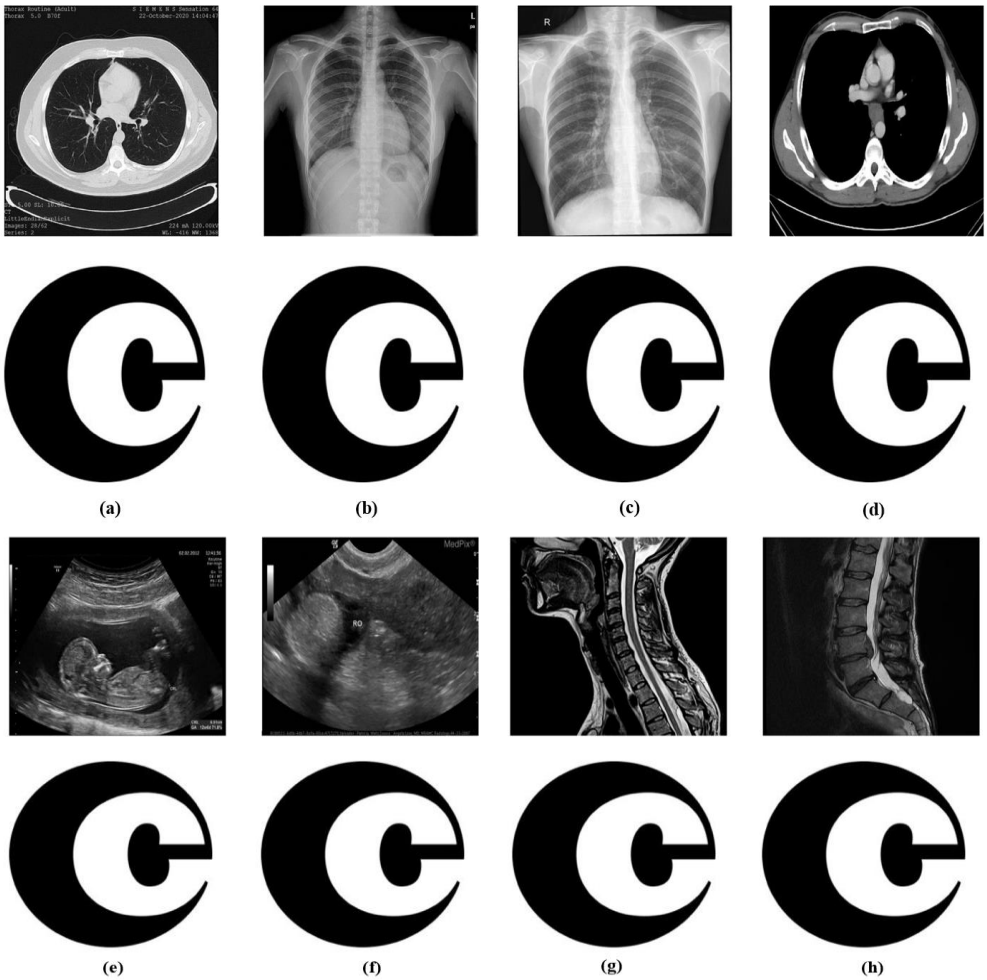

Figure 7. Watermarked images with corresponding extracted watermarks (no attack)

Table 1. PSNR and SSIM measurements for diverse watermarked images

Image	Modality	PSNR	SSIM
Chest1_X-ray	X-ray	64.32	0.9999
Chest2_X-ray		64.27	0.9999
Thoracic1_CT	CT	64.56	1.0000
Thoracic2_CT		64.33	1.0000
Lumbar_MRI	MRI	64.20	0.9999
Spinal_MRI		64.37	1.0000
Ovarian_Ultrasound	Ultrasound	64.55	0.9999
Fetal_Ultrasound		64.67	1.0000

Table 2. Assessment of imperceptibility performance across varying parameter settings (host images and watermarks of different dimensions)

Cover Medical Image	Watermark	Watermark Size 256 × 256			Watermark Size 128 × 128			Watermark Size 64 × 64		
		PSNR	SSIM	NC	PSNR	SSIM	NC	PSNR	SSIM	NC
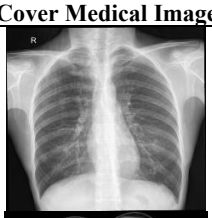		58.78	0.9995	1.0000	59.54	0.9997	1.0000	63.00	0.9999	0.9999
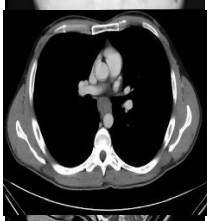		61.70	0.9999	1.0000	66.56	1.0000	1.0000	68.28	1.0000	1.0000
		64.37	1.0000	1.0000	65.31	1.0000	1.0000	68.90	1.0000	1.0000
		57.98	0.9998	1.0000	58.37	0.9998	1.0000	61.31	0.9999	0.9999

Figure 7 demonstrates that both the watermarked image and the extracted watermark retain excellent visual quality, validating the efficiency of the proposed method. PSNR and SSIM measurements for various categories of watermarked medical images are displayed in Table 1, together with NC values for the recovered watermarks. The peak PSNR and SSIM values attained were 64.67 and 1.0000, respectively. These metrics reflect superior visual transparency and strong resemblance between original images and their watermarked versions. Additionally, the elevated NC values (NC=1.0000) validate the extraction algorithm's robust performance.

Imperceptibility results obtained through extensive experimentation using different host images and varied watermarks (W_a-W_e) with multiple dimensions (256×256, 128×128 and 64×64) are presented in Table 2. The findings indicate that the watermarked images and their corresponding extracted watermarks consistently exhibit high visual quality. Moreover, the embedded watermarks remain fully imperceptible, preserving the original image content. Quantitative evaluation further supports this observation, with PSNR values exceeding 57.98dB and SSIM and NC scores greater than 0.9999, thereby confirming the strong invisibility performance of the proposed approach.

5.3 Effect of payload size on watermarked image imperceptibility and robustness

The embedding capacity significantly affects watermarked image quality when tested on eight medical images from different modalities with payloads between 0.1 and 2 BPP. As illustrated in Figure 8 the PSNR decreases steadily from 85dB at 0.1 BPP to 58dB at 2 BPP, showing that image quality reduces as more data is embedded. However, the SSIM remains consistently high, dropping only slightly from 0.99998 to 0.99975, which indicates that the visual appearance and structure of the medical images are well preserved across all modalities tested. The NCC values show initial improvement from 0.1 BPP to around 1.0 BPP before stabilizing above 0.9999975, suggesting good correlation maintenance between original and watermarked images. These findings demonstrate that despite the PSNR reduction, the watermarking method maintains excellent visual quality and structural integrity across different medical imaging types. The results indicate that embedding capacities between 1.0-2.0 BPP provide a practical balance, offering sufficient space for patient data while preserving the diagnostic quality essential for medical applications across various imaging modalities.

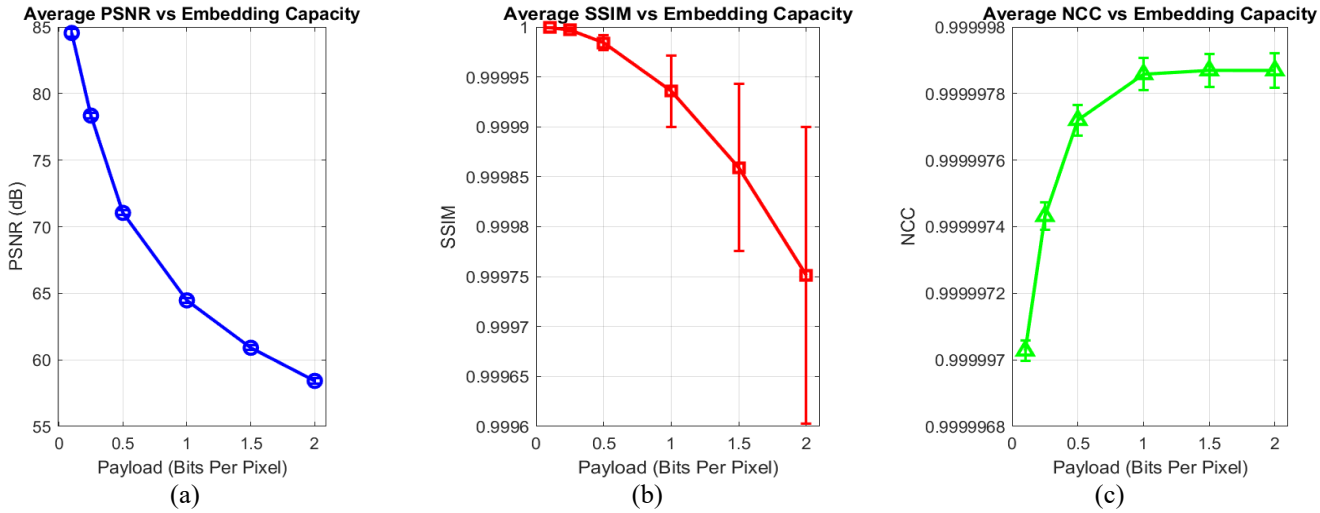

Figure 8. Effect of payload size on watermarked image imperceptibility and robustness

5.4 The computational complexity

The computational cost of the presented DTCWT-DCT-SVD watermarking framework primarily stems from the DTCWT, the 2D-DCT, and the SVD. For a host image of size M×M, a single-level DTCWT requires $O(M^2)$ operations, while DCT2 on the high-frequency subband adds O (M^2 log M). The subsequent SVD contributes $O(M^3)$ in the worst case, though the effective cost is reduced since it is applied to smaller subband blocks (e.g., 256 × 256). Embedding and extraction involve modifying singular values linearly with the watermark length L, i.e., O(L). Overall, the scheme has a dominant complexity of approximately $O(M^3)$.

In practice, the method was implemented in MATLAB R2022b on a desktop computer with an Intel Core i5-6th CPU (3.2GHz) and 8GB RAM. For 512 × 512 medical images, the average embedding time was 1.6035s, while extraction required 1.1405s (Table 3).

These results demonstrate that the DTCWT-DCT-SVD algorithm is highly efficient, provides excellent imperceptibility and robustness, and is well-suited for secure medical image transmission. Further speedups can be obtained via GPU parallelization or optimized compiled languages.

Table 3. Computational duration measurements for medical image samples

Medical Images	Embedding Time (Sec.)	Extraction Time (Sec.)	Total Time (Sec.)
Thoracic1_CT	0.2170	0.1404	0.3574
Spinal_MRI	0.1997	0.1419	0.3416
Chest1_X-ray	0.1989	0.1459	0.3448
Thoracic2_CT	0.1972	0.1425	0.3397
Lumbar_MRI	0.1977	0.1412	0.3389
Chest2_X-ray	0.1971	0.1429	0.3400
Ovarian_Ultrasound	0.1984	0.1416	0.3400
Fetal_Ultrasound	0.1975	0.1441	0.3416
The average	1.6035	1.1405	2.744

5.5 Robustness analysis

In medical imaging applications, where diagnostic precision directly affects patient treatment decisions, ensuring image authenticity and integrity represents a fundamental requirement. Protecting these critical data assets from unauthorized modifications or attacks is therefore essential for maintaining clinical reliability. Once imperceptibility benchmarks are satisfied, thorough robustness validation through systematic attack testing becomes necessary. To establish system robustness, watermark extraction capability is evaluated across a comprehensive attack spectrum. The robustness evaluation encompasses 23 distinct attack scenarios organized into six primary categories. Geometric transformations include rotation, rescaling, directional flipping, cropping, and translation operations. Signal processing attacks involve sharpening, Gaussian LP filtering, Wiener filtering, average filtering, and median filtering techniques. Noise contamination testing employs speckle, Gaussian, and salt-and-pepper noise variants. Compression-based attacks utilize both JPEG and JPEG2000 standards. Image adjustment testing focuses on histogram equalization, while content manipulation assessment includes copy-paste operations. System robustness assessment relies on calculating the (NC) coefficient between the original and extracted watermarks. An NC threshold of 0.75 or above is generally considered acceptable for determining successful watermark recovery [32].

Table 4 details the robustness evaluation for Lumbar_MRI/Wc set to gain factor =0.6, where the system's robustness was tested against various image processing and geometric attacks across three watermark sizes: 256×256, 128×128, and 64×64. The watermarking system demonstrates exceptional robustness with NC values consistently exceeding 0.9999 across all sizes. Perfect recovery (NC = 1.0000) occurs for rotation (2°), rescaling (2), cropping (2%), and sharpening attacks across all watermark sizes. Near-perfect performance (NC ≥ 0.9999) is achieved for speckle noise, Gaussian noise, JPEG 2000 compression, JPEG compression (QF = 50), Gaussian LPF, Wiener filter, and median filter attacks.

Geometric attacks show strong resilience, with 45° rotation maintaining NC values of 0.9999-0.99998 across different sizes. Salt and pepper noise demonstrates robust performance with NC values ranging from 0.99995-0.99999. Motion blur and histogram equalization preserve strong performance, with NC values of 0.99991-0.99999 and 0.99991-0.99997 respectively. Average filtering shows the most variation across sizes, with NC values ranging from 0.99993 (64 × 64) to 0.99999 (256×256). Overall, watermark size impact is minimal, with even the smallest 64×64 watermarks maintaining NC values above 0.99991, indicating consistent scale-invariant performance across all payload sizes.

To further evaluate the resilience of the proposed watermarking methodology, supplementary testing with different parameter configurations across various attack scenarios has been performed using the "Thoracic2_CT" host image (512 × 512 pixels) and the "W_e" watermark (256 × 256 pixels). The obtained outcomes are presented in Table 5. Translation (dx = -30, dy = -90), flip direction, and copy-paste operations achieve perfect recovery (NC = 1.0000), demonstrating complete resilience to geometric transformations and content manipulation. Noise attacks show strong performance: Gaussian noise (Var = 0.05) yields NC = 0.99902, salt and pepper noise achieves NC = 0.99944, and speckle noise demonstrates highest resilience with NC = 0.99975. The extracted watermark images confirm successful recovery across all attacks, with the "LTSS" logo remaining clearly visible and recognizable.

Table 4. Watermarking system robustness under various attacks: Lumbar_MRI with W_c at alpha = 0.6

Attack	NC Values		
	Watermark Size 256 × 256	Watermark Size 128 × 128	Watermark Size 64 × 64
Rotation (2°)	1.0000	0.99999	0.99998
Rotation (45°)	0.99998	0.9999	0.99971
Rescaling (0.5)	0.99999	0.99996	0.99993
Rescaling (2)	1.0000	0.99999	0.99997
Cropping 2%	1.0000	0.99999	0.99999
Sharpening 0.8	1.0000	1.0000	1.0000
Speckle noise (var =0.001)	1.0000	1.0000	0.99999
Gaussian noise (var =0.001)	0.99998	0.99996	0.9999
Salt and peppers noise (var =0.001)	0.99999	0.99998	0.99995
Motion blur (θ=7, L=3)	0.99999	0.99997	0.99994
Histogram equalization	0.99999	0.99997	0.99991
JPEG 2000 compression (CR=12)	1.0000	0.99999	0.99998
JPEG Compression (QF=50)	1.0000	0.99999	0.99999
Gaussian LPF (3×3)	0.99999	0.99996	0.99992
Wiener filter (3×3)	1.0000	0.99999	0.99998
Average filter (3×3)	0.99999	0.99997	0.99993
Median filter (3×3)	1.0000	0.99999	0.99998

Table 5. Extracted watermark samples under multiple attack types at alpha =0.6

Translation (dx = -30, dy = -90)	**Flip Direction**	**Copy Paste**
NC = 1.0000	NC = 1.0000	NC = 1.0000
Translated Image (dx=-30, dy=-90)	Flipped Image (Horizontal)	Copy-Paste Attacked Image
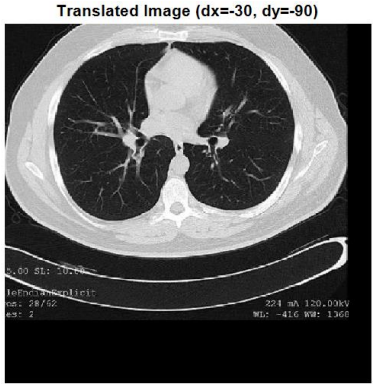	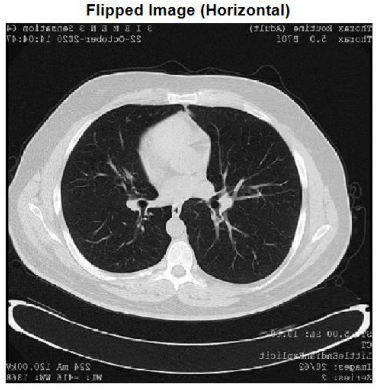	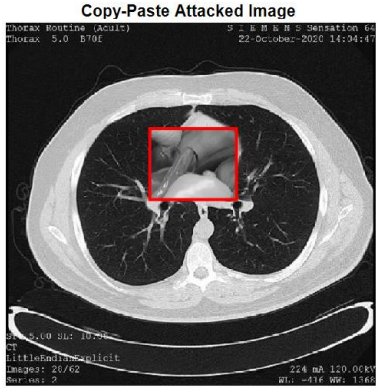
Extracted Watermark after Translation Attack	Extracted Watermark after Horizontal Flip Attack	Extracted Watermark after Copy-Paste Attack
NC = 1.0000	NC = 1.0000	NC = 1.0000
	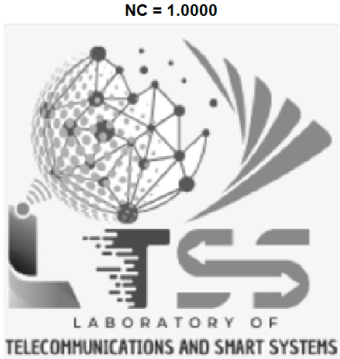	

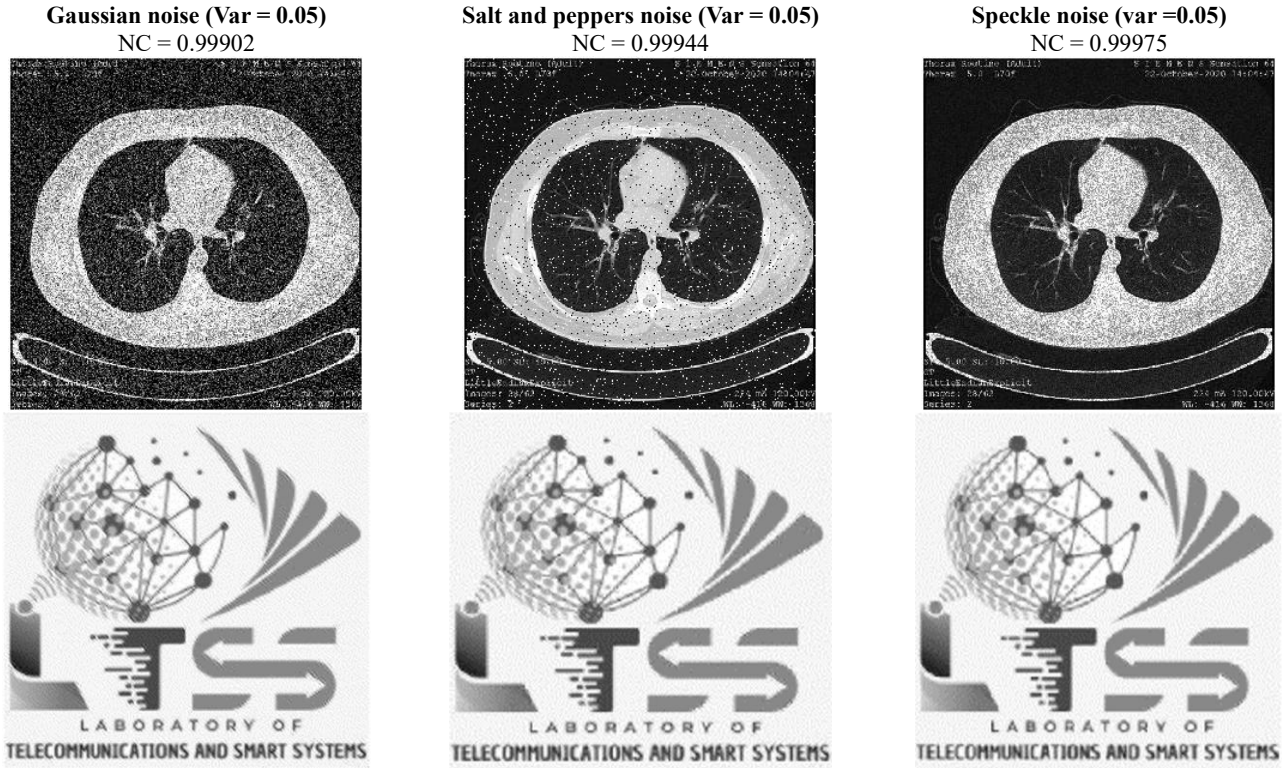

5.6 Comparison of performance with other schemes

To assess the proposed watermarking method's performance, a comparative analysis is conducted against current leading techniques from recent research. The evaluation focuses on highlighting the strengths and weaknesses of our approach compared to existing methods, with particular emphasis on visual quality preservation and robustness against various attacks—critical requirements for effective copyright protection and image verification. Fair comparison is ensured through standardized testing using identical cover images and watermark data across all evaluated methods. The evaluation dataset comprises diverse medical imaging modalities at 512×512 pixel resolution, with embedded watermark (W_c) at 256×256 pixel dimensions.

Table 6 compares PSNR values of the proposed method against four recent watermarking techniques across different medical images. The proposed method achieves consistently superior performance with PSNR values ranging from 64.20-64.67dB across all tested modalities (X-ray, CT, MRI, and US images), representing improvements of approximately 15-21dB over competing methods. The existing techniques show lower performance, with Awasthi and Srivastava [30] achieving 42.90-42.96dB, Latreche et al. [7] demonstrating 42.99-43.04dB, and Chaudhary et al. [46] showing 48.95-49.61dB. This substantial improvement of approximately 15-21dB indicates the proposed method's superior ability to preserve diagnostic image quality while embedding watermarks, demonstrating its effectiveness for medical image watermarking applications where maintaining visual fidelity is critical.

Table 7 presents a robustness comparison between the proposed method and four existing approaches based on Normalized Correlation (NC) values under different attack conditions. NC values closer to 1.0 indicate better watermark recovery after attacks. The proposed method exhibits outstanding robustness, achieving perfect NC values of 1.0000 for most attacks, including rotation, rescaling (factor 2), cropping, sharpening, speckle noise, JPEG compression variants, Wiener filter, and median filter, while maintaining NC values above 0.99999 for rescaling (0.5), salt and pepper noise, Gaussian noise, motion blur, histogram equalization, and Gaussian low-pass filter. This consistent performance indicates excellent resilience against both geometric and signal processing attacks. In contrast, competing methods show significant vulnerabilities to specific attacks. Notably, Awasthi and Srivastava [30] and another variant [30] exhibit sharp performance degradation under histogram equalization (NC $\approx$ 0.71), while Latreche et al. [7] show reduced performance (NC=0.8571). The existing methods also demonstrate lower performance under rotation attacks, with Awasthi and Srivastava [30] achieving NC values of 0.7502 and 0.7625, compared to the proposed method's perfect 1.0000. Chaudhary et al. [46] show moderate performance where data is available but has limited coverage across attack types (marked as N/A for many scenarios). This comprehensive superiority across diverse attack types validates the proposed framework's enhanced robustness for practical watermarking applications.

Table 6. Comparative PSNR analysis: Proposed scheme vs. Awasthi and Srivastava [30], Latreche et al. [7], and Chaudhary et al. [46]

Test Medical Images	[30]	[30]	[7]	[45]	Our Method
X-ray image	42.92	42.96	43.04	48.98	64.32
CT image	43.77	43.82	43.89	49.61	64.33
MRI image	42.91	42.90	42.99	49.60	64.20
US image	43.04	43.16	43.03	48.95	64.67

Table 7. Comparative NC analysis: Proposed scheme vs. Awasthi and Srivastava [30], Boubakeur et al. [7], and Chaudhary et al. [46]

Attack	NC Values				
	[7]	[30]	[30]	[46]	Our Proposed
Rotation (2°)	0.9926	0.7502	0.7625	N/A	1.0000
Rescaling (0.5)	0.9998	0.9995	0.9995	N/A	0.99999
Salt and peppers noise (var=0.001)	0.9997	0.9911	0.9931	0.98	0.99999
Rescaling (2)	0.9998	0.9995	0.9995	N/A	1.0000
Speckle noise (var=0.001)	0.9997	0.9992	0.9993	0.98	1.0000
Cropping 2%	0.9994	0.7324	0.7984	N/A	1.0000
Sharpening 0.8	0.9991	0.9922	0.9948	0.97	1.0000
Gaussian noise (var=0.001)	0.9995	0.9734	0.9822	N/A	0.99998
Motion blur (θ=7, L=3)	0.9703	0.9483	0.9697	N/A	0.99999
JPEG Compression (QF=50)	0.9984	0.9947	0.9947	0.96	1.0000
Histogram equalization	0.8571	0.7142	0.7133	N/A	0.99999
JPEG 2000 compression (CR=12)	0.9980	0.9993	0.9993	0.99	1.0000
Gaussian low pass filter (3×3)	0.9980	0.9995	0.9995	0.53	0.99999
Wiener filter (3×3)	0.9929	0.9881	0.9928	N/A	1.0000
Average filter (3×3)	0.9476	0.9178	0.9457	0.51	0.99999
Median filter (3×3)	0.9819	0.9799	0.9888	0.90	1.0000

6. CONCLUSIONS

This study presents a robust watermarking framework for medical images integrating DTCWT, DCT, and SVD transforms. The method achieves excellent performance with PSNR of 64.20-64.67dB across X-ray, CT, MRI, and ultrasound images, SSIM above 0.9992, and NC values consistently exceeding 0.99999 with perfect recovery for most attacks. Comparative analysis shows 15-21dB improvements over existing techniques, demonstrating superior robustness against various attack scenarios while preserving diagnostic quality.

Despite these promising results, several limitations remain. Extreme distortions such as severe cropping or very high noise levels can still reduce watermark recovery quality. Embedding capacity was evaluated up to 2 BPP; higher payloads may compromise visual fidelity. Moreover, the current evaluation relies on objective image quality metrics (PSNR, SSIM, NC), while clinical validation through radiologist assessment is yet to be performed.

Future work will address these aspects by developing reversible watermarking schemes for lossless recovery, extending the method to real-time video watermarking for telemedicine, and incorporating diagnostic quality assessments in collaboration with medical experts. These directions will further strengthen the framework's practicality and reliability for secure healthcare applications.

ACKNOWLEDGMENT

Princess Nourah bint Abdulrahman University Researchers Supporting Project number (PNURSP2025R754), Princess Nourah bint Abdulrahman University, Riyadh, Saudi Arabia

REFERENCES

[1] Naima, S., Boukhamla, A.Z.E., Narima, Z., Amine, K., Redouane, K.M., Sahu, A.K. (2025). Secure and imperceptible frequency-based watermarking for medical images. Circuits, Systems, and Signal Processing, 44(1): 196-217. https://doi.org/10.1007/s00034-024-02814-y

[2] Khaldi, A., Redouane, K.M., Bilel, M. (2023). A medical image watermarking system based on redundant wavelets for secure transmission in telemedicine applications. Wireless Personal Communications, 132(2): 823-839. https://doi.org/10.1007/s11277-023-10636-5

[3] Hurrah, N.N., Parah, S.A., Sheikh, J.A., Al-Turjman, F., Muhammad, K. (2019). Secure data transmission framework for confidentiality in IoTs. Ad Hoc Networks, 95: 101989. https://doi.org/10.1016/j.adhoc.2019.101989

[4] Khare, P., Srivastava, V.K. (2021). A reliable and secure image watermarking algorithm using homomorphic transform in DWT domain. Multidimensional Systems and Signal Processing, 32(1): 131-160. https://doi.org/10.1007/s11045-020-00732-1

[5] Wazirali, R., Ahmad, R., Al-Amayreh, A., Al-Madi, M., Khalifeh, A. (2021). Secure watermarking schemes and their approaches in the IoT technology: An overview. Electronics, 10(14): 1744. https://doi.org/10.3390/electronics10141744

[6] Sahu, A.K., Sahu, M., Patro, P., Sahu, G., Nayak, S.R. (2023). Dual image-based reversible fragile watermarking scheme for tamper detection and localization. Pattern Analysis and Applications, 26(2): 571-590. https://doi.org/10.1007/s10044-022-01104-0

[7] Latreche, B., Merrad, A., Benziane, A., Naimi, H., Saadi, S. (2024). A robust dual-layer medical image watermarking scheme based on matrix factorization in the LWT domain for E-healthcare applications. Multimedia Tools and Applications, 84: 29883-29913. https://doi.org/10.1007/s11042-024-20331-7

[8] Bouarroudj, R., Souami, F., Bellala, F.Z., Zerrouki, N., Harrou, F., Sun, Y. (2025). Secure and reversible fragile watermarking for accurate authentication and tamper localization in medical images. Computers and Electrical Engineering, 123: 110072. https://doi.org/10.1016/j.compeleceng.2025.110072

[9] Laouamer, L. (2023). Toward a robust image watermarking method: Exploiting human visual system properties in the spatial domain. Traitement du Signal, 40(3): 1119-1126. https://doi.org/10.18280/ts.400327

[10] Jana, M., Jana, B., Joardar, S. (2023). A novel approach of fragile watermarking for authentication and tamper detection exploiting Local Binary Pattern (LBP). In International Conference on Computational Intelligence in Communications and Business Analytics, pp. 3-16. https://doi.org/10.1007/978-3-031-48879-5_1

[11] Srinadh, V., Maram, B., Daniya, T. (2022). Dual image-based high quality digital image watermarking. In Smart Technologies for Power and Green Energy: Proceedings of STPGE 2022, pp. 169-177. https://doi.org/10.1007/978-981-19-2764-5_14

[12] De, S., Maity, S., Bhaumik, J., Pal, P., Giri, D. (2024). Spread-spectrum based a new secured robust image watermarking scheme. In International Conference on Network Security and Blockchain Technology. Singapore: Springer Nature Singapore, pp. 73-87. https://doi.org/10.1007/978-981-97-8051-8_7

[13] Elhossiny, M.A., Elghazawy, M.A.I., Miled, A.B., Mahmoud, A.F., Abdalla, F.A., Nawaz, M.A. (2025). Intermediate significant bits embedding for telemedicine applications. Journal of Integrated Science and Technology, 13(5): 1111. https://doi.org/10.62110/sciencein.jist.2025.v13.1111

[14] Yaswanth, M., Shashidhar, B., Dharwadkar, N.V., Ali, S. T. (2025). Enhanced pixel value differencing in YCbCr for high-capacity. In 2025 International Conference on Innovations in Intelligent Systems: Advancements in Computing, Communication, and Cybersecurity (ISAC3), Bhubaneswar, India, pp. 1-5. https://doi.org/10.1109/ISAC364032.2025.11156340

[15] Benoraira, A., Benmahammed, K., Boucenna, N. (2015). Blind image watermarking technique based on differential embedding in DWT and DCT domains. EURASIP Journal on Advances in Signal Processing, 2015(1): 55. https://doi.org/10.1186/s13634-015-0239-5

[16] Alrammahi, A., Sajedi, H. (2025). Robust image watermarking based on DWT and RDWT combined with Möbius transformations. Available at SSRN 4981189. https://doi.org/10.2139/ssrn.4981189

[17] Rijati, N., Ghosal, S.K., Sahu, A.K., Sambas, A., Ignatius Moses Setiadi, D.R. (2025). DWT-DCT image watermarking with quantum-inspired optimization. International Journal of Intelligent Engineering & Systems, 18(1): 1034. https://doi.org/10.22266/ijies2025.0229.74

[18] Sabeti, V. (2025). An enhanced DWT-SVD-based robust image watermarking scheme optimized for imperceptibility and robustness. Arabian Journal for Science and Engineering, 50: 15529-15550. https://doi.org/10.1007/s13369-024-09917-3.

[19] Athimoolam, A.K., Chevula, C.K. (2025). A novel digital watermarking technique empowered by MWT and DCT fusion with high resilience against cropping attacks. Annals of Telecommunications. https://doi.org/10.1007/s12243-025-01078-0

[20] Jana, S., Pal, P., Mahadani, A.K., Chowdhuri, P., Giri, D. (2024). LWT-based watermarking scheme for image authentication. Proceedings of International Conference on Network Security and Blockchain Technology, 1158: 47-57. https://doi.org/10.1007/978-981-97-8051-8_5

[21] Patsariya, S., Dixit, M. (2022). A new block based non-blind hybrid color image watermarking approach using lifting scheme and chaotic encryption based on Arnold cat map. Traitement du Signal, 39(4): 1159-1168. https://doi.org/10.18280/ts.390408

[22] Alshoura, W.H., Alawida, M. (2025). Secure and flexible image watermarking using IWT, SVD, and chaos models for robustness and imperceptibility. Scientific Reports, 15(1): 7231. https://doi.org/10.1038/s41598-025-91876-2

[23] Wahyudi, M.I., Fauzi, I., Atmojo, D. (2025). Robust image watermarking based on hybrid IWT-DCT-SVD. IJACI: International Journal of Advanced Computing and Informatics, 1(2): 89-98. https://doi.org/10.71129/ijaci.v1.i2.pp89-98

[24] Lebcir, M., Awang, S., Benziane, A. (2024). Robust blind image watermarking scheme using a modified embedding process based on differential method in DTCWT-DCT. Multimedia Tools and Applications, 83(22): 61379-61405. https://doi.org/10.1007/s11042-024-18185-0

[25] Tajamal, K., Nizami, I. F., Majid, M. (2025). Blind image quality assessment in JPEG compressed domain. In 2025 International Conference on Emerging Technologies in Electronics, Computing, and Communication (ICETECC), Jamshoro, Pakistan, pp. 1-5. https://doi.org/10.1109/ICETECC65365.2025.11071248

[26] Sundhararaj, V., Meenakshipriya, B., Devi, P.N., Vignesh, K.E. (2025). DWT-DCT-SVD: A hybrid image watermarking algorithm with FPP resistant enhancement. Circuits, Systems, and Signal Processing, 44: 6650-6675. https://doi.org/10.1007/s00034-025-03097-7

[27] Sayah, M.M., Narima, Z., Amine, K., Redouane, K.M. (2024). Integer wavelet transform based data hiding scheme for electrocardiogram signals protection. International Journal of Computational Science and Engineering, 27(3): 364-376. https://doi.org/10.1504/IJCSE.2024.138419

[28] Basit, A., Toor, W.T., Saadi, M., Maroof, N., Khan, S. A., Otaibi, S.A. (2023). Reversible encryption and lossless data hiding for medical imaging aiding smart health care. Cluster Computing, 26(5): 2977-2991. https://doi.org/10.1007/s10586-022-03792-z

[29] Shubuh, S., Ernawan, F., Amrullah, A., Wahyu, P. (2024). Robust image watermarking based on IWT-DCT-SVD for copyright protection. Iraqi Journal for Computer Science and Mathematics, 5(4): 3. https://doi.org/10.52866/2788-7421.1201

[30] Awasthi, D., Srivastava, V.K. (2022). LWT-DCT-SVD and DWT-DCT-SVD based watermarking schemes with their performance enhancement using jaya and particle swarm optimization and comparison of results under various attacks. Multimedia Tools and Applications, 81(18): 25075-25099. https://doi.org/10.1007/s11042-022-12456-4

[31] Fares, K., Khaldi, A., Redouane, K., Salah, E. (2021). DCT & DWT based watermarking scheme for medical information security. Biomedical Signal Processing and Control, 66: 102403. https://doi.org/10.1016/j.bspc.2020.102403

[32] Anand, A., Singh, A.K. (2020). An improved DWT-SVD domain watermarking for medical information security. Computer Communications, 152: 72-80. https://doi.org/10.1016/j.comcom.2020.01.038

[33] Kanwal, S., Tao, F., Taj, R., Abbas, Q., Amin, F. (2025). Discrete cosine transform and discrete wavelet transform

based hybrid method for robust and blind medical image watermarking. Peer-to-Peer Networking and Applications, 18(5): 251. https://doi.org/10.1007/s12083-025-02059-9

[34] Kingsbury, N. (2001). Complex wavelets for shift invariant analysis and filtering of signals. Applied and Computational Harmonic Analysis, 10(3): 234-253. https://doi.org/10.1006/acha.2000.0343

[35] Zebbiche, K., Khelifi, F., Loukhaoukha, K. (2018). Robust additive watermarking in the DTCWT domain based on perceptual masking. Multimedia Tools and Applications, 77(16): 21281-21304. https://doi.org/10.1007/s11042-017-5451-x

[36] Coria, L.E., Pickering, M.R., Nasiopoulos, P., Ward, R.K. (2008). A video watermarking scheme based on the dual-tree complex wavelet transform. IEEE Transactions on Information Forensics and Security, 3(3): 466-474. https://doi.org/10.1109/TIFS.2008.927421

[37] Bouarroudj, R., Souami, F., Bellala, F.Z., Zerrouki, N. (2024). A reversible fragile watermarking technique using fourier transform and fibonacci Q-matrix for medical image authentication. Biomedical Signal Processing and Control, 92: 105967. https://doi.org/10.1016/j.bspc.2024.105967

[38] Zermi, N., Khaldi, A., Kafi, M.R., Kahlessenane, F., Euschi, S. (2021). Robust SVD-based schemes for medical image watermarking. Microprocessors and Microsystems, 84: 104134. https://doi.org/10.1016/j.micpro.2021.104134

[39] Teoh, Y.J., Ling, H.C., Wong, W.K., Chew, I.M., Basuki, T.A., Karim, H.A. (2025). A robust SVD-based watermarking scheme using orthogonal vectors and PSO-enhanced scaling factor. Cluster Computing, 28(13): 850. https://doi.org/10.1007/s10586-025-05581-w

[40] Nouioua, N., Seddiki, A., Ghaz, A. (2020). Blind digital watermarking framework based on DTCWT and NSCT for telemedicine application. Traitement du Signal, 37(6): 955-964. https://doi.org/10.18280/ts.370608

[41] Singh, S., Singh, R., Singh, A.K., Siddiqui, T.J. (2017). SVD-DCT based medical image watermarking in NSCT domain. In Quantum Computing: An Environment for Intelligent Large Scale Real Application, 33: 467-488. https://doi.org/10.1007/978-3-319-63639-9_20

[42] The National Library of Medicine presents MedPix. https://medpix.nlm.nih.gov/home, accessed on Sep. 4, 2025.

[43] COVID-19 Radiography Database. https://www.kaggle.com/datasets/tawsifurrahman/covid19-radiography-database, accessed on Feb. 27, 2025.

[44] Naffouti, S.E., Kricha, A., Sakly, A. (2023). A sophisticated and provably grayscale image watermarking system using DWT-SVD domain. The Visual Computer, 39(9): 4227-4247. https://doi.org/10.1007/s00371-022-02587-y

[45] Sun, Y., Su, Q., Chen, S., Zhang, X. (2022). A double-color image watermarking algorithm based on quaternion Schur decomposition. Optik, 269: 169899. https://doi.org/10.1016/j.ijleo.2022.169899

[46] Chaudhary, H., Garg, P., Vishwakarma, V.P. (2025). Enhanced medical image watermarking using hybrid DWT-HMD-SVD and Arnold scrambling. Scientific Reports, 15(1): 9710. https://doi.org/10.1038/s41598-025-94080-4